Detection of gravitational wave mixed polarization with single space-based detectors

Chao Zhang,[1,*] Yungui Gong,[1,†] Dicong Liang,[2,1,‡] and Chunyu Zhang[1,§]

[1]*School of Physics, Huazhong University of Science and Technology, Wuhan, Hubei 430074, China*
[2]*Kavli Institute for Astronomy and Astrophysics, Peking University, Beijing 100871, China*

(Received 21 September 2021; accepted 3 May 2022; published 27 May 2022)

General Relativity predicts only two tensor polarization modes for gravitational waves while at most six possible polarization modes are allowed in the general metric theory of gravity. The number of polarization modes is determined by the specific modified theory of gravity. Therefore, the determination of polarization modes can be used to test gravitational theory. We introduce a concrete data analysis pipeline for a space-based detector such as LISA to detect the polarization modes of gravitational waves. This method can be used for monochromatic gravitational waves emitted from any compact binary system with a known sky position and frequency to detect mixtures of tensor and extra polarization modes. We use the source J0806.3 + 1527 with one year of simulation data as an example to show that this approach is capable of probing pure and mixed polarizations without knowing the exact polarization modes. We also find that the ability of detection of extra polarization depends on the gravitational-wave source location and the amplitude of nontensorial components.

DOI: 10.1103/PhysRevD.105.104062

I. INTRODUCTION

So far there have been multiple confirmed gravitational wave (GW) detections [1–14] since the first GW event GW150914 observed by the Laser Interferometer Gravitational-Wave Observatory (LIGO) scientific Collaboration, and the Virgo Collaboration [1,2]. Distinguishing GW polarizations is extremely useful to perform tests about the validity of General Relativity (GR). The transient GWs detected by ground-based GW detectors are the merging signals with the duration of seconds to minutes in the frequency band around several hundred hertz, so it is impossible to measure the signals' polarization contents with advanced LIGO alone because the two detectors are nearly co-oriented [15,16] and the observed signals are so short that we can ignore the motion of the detector around the Sun. However, some preliminary results on the signals' polarization contents were obtained with the LIGO-Virgo network [5,8,13,17]. In general metric theory of gravity, GWs can have up to six polarization modes [18,19]: two transverse-traceless tensor modes ($+$ and $\times$), two vector modes (x and y), a scalar breathing mode (b), and a scalar longitudinal mode (l). The specific modified theory of gravity uniquely determines the polarization modes. For example, in Brans-Dicke theory [20] there exists one extra breathing mode beyond the two transverse-traceless tensor modes of GR. The scalar polarization mode is a mixture of breathing mode and longitudinal mode if the scalar field is massive in the generic scalar-tensor theory of gravity [21–24]. Einstein-Æther theory [25] predicts the existence of scalar and vector polarization modes [24,26,27] while generalized tensor-vector-scalar theories, such as TeVeS theory [28], predict the existence of all six polarization modes [24]. Therefore, the detection of extra polarization modes allows us to falsify GR. To separate the polarization modes of GWs, in principle, the number of ground-based GW detectors oriented differently should be equal to or larger than the number of the polarization modes. The network of ground-based GW detectors including advanced LIGO [15,16], advanced Virgo [29], KAGRA [30,31], and LIGO India has the ability of probing extra polarization modes [32–34]. In past years, different methods were developed to probe nontensorial polarizations in stochastic GW backgrounds [35–38], continuous GWs [39–42], GW bursts [43,44], and GWs from compact binary coalescences [45,46]. In particular, the Fisher information matrix approximation was usually used to estimate the parameters of the source and to discuss the measurement of polarization modes [46–62].

For stellar or intermediate black hole binaries with the mass range $10^4\ M_\odot - 10^4\ M_\odot$, in the early inspiral phase the GW frequency is in the mHz range and its evolution can be neglected during the mission of the space-based GW detector. The proposed space-based GW observatories

*chao_zhang@hust.edu.cn
†Corresponding author.
yggong@hust.edu.cn
‡dcliang@pku.edu.cn
§chunyuzhang@hust.edu.cn

including LISA [63,64], TianQin [65], and Taiji [66] can detect the monochromatic GW signals emitted by these wealthy sources. Due to the orbital motion of the detector in space, along its trajectory the single detector can be effectively regarded as a set of virtual detectors and therefore form a virtual network to measure the polarization contents of the monochromatic GW signals. By taking a specific linear combination of the outputs in the network of detectors it is possible to remove any tensorial signal present in the data [67,68]. A particular χ^2 distribution is followed by the null energy constructed with this method [68] when the null energy is calculated at the true sky position. If nontensorial polarization exists in the data, then the null energy evaluated at the true sky position no longer follows the particular χ^2 distribution [34]. Based on these results, we introduce one concrete data-analysis pipeline to check for the existence of extra polarization for a single space-based GW detector. Apart from being able to detect mixtures of tensor polarization modes and alternative polarization modes, this method has the added advantage that no waveform model is needed, and monochromatic GWs from any kind of compact binary systems with known sky positions and frequencies can be used.

The paper is organized as follows. In Sec. II, we describe the basics of the GW signal registered in the space-based GW detector. In Sec. III, we present general monochromatic waveforms including extra polarization modes and construct the method to discover alternative polarization modes. We then apply the method on the source J0806.3 + 1527 with one year of simulation data for LISA, Taiji, and TianQin. Our conclusion and discussion are presented in Sec. IV.

II. GRAVITATIONAL-WAVE SIGNAL

It is convenient to describe GWs and the motion of space-based GW detectors like LISA, TianQin, and Taiji in the heliocentric coordinate system with the constant basis vectors $\{\hat{e}_x, \hat{e}_y, \hat{e}_z\}$ [69]. For GWs propagating in the direction $\hat{\omega}$, we introduce a set of unit vectors $\{\hat{\theta}, \hat{\phi}, \hat{\omega}\}$ which are perpendicular to each other,

$$\begin{aligned}
\hat{\theta} &= \cos(\theta)\cos(\phi)\hat{e}_x + \cos(\theta)\sin(\phi)\hat{e}_y - \sin(\theta)\hat{e}_z,\\
\hat{\phi} &= -\sin(\phi)\hat{e}_x + \cos(\phi)\hat{e}_y,\\
\hat{\omega} &= -\sin(\theta)\cos(\phi)\hat{e}_x - \sin(\theta)\sin(\phi)\hat{e}_y - \cos(\theta)\hat{e}_z,
\end{aligned} \tag{1}$$

where the angles (θ, ϕ) are the angular coordinates of the source. To describe the six possible polarization modes of GWs in general metric theory of gravity, the polarization angle ψ is introduced to form polarization axes of the gravitational radiation,

$$\hat{p} = \cos\psi\hat{\theta} + \sin\psi\hat{\phi}, \qquad \hat{q} = -\sin\psi\hat{\theta} + \cos\psi\hat{\phi}. \tag{2}$$

The polarization tensors are

$$\begin{aligned}
e^{+}_{ij} &= \hat{p}_i\hat{p}_j - \hat{q}_i\hat{q}_j, \qquad e^{\times}_{ij} = \hat{p}_i\hat{q}_j + \hat{q}_i\hat{p}_j,\\
e^{x}_{ij} &= -\hat{p}_i\hat{\omega}_j - \hat{\omega}_i\hat{p}_j, \qquad e^{y}_{ij} = -\hat{q}_i\hat{\omega}_j - \hat{\omega}_i\hat{q}_j,\\
e^{l}_{ij} &= \sqrt{2}\hat{\omega}_i\hat{\omega}_j, \qquad e^{b}_{ij} = \hat{p}_i\hat{p}_j + \hat{q}_i\hat{q}_j,
\end{aligned} \tag{3}$$

where $+$ and $\times$ denote two transverse-traceless tensor modes, x and y denote two vector modes, b denotes the scalar breathing mode, and l denotes the scalar longitudinal mode. In terms of the six polarization tensors e^A_{ij}, GWs in general metric theory of gravity have the form

$$h_{ij}(t) = \sum_A e^A_{ij} h_A(t), \tag{4}$$

where $A = +, \times, x, y, l, b$.

For a monochromatic GW with the frequency f propagating along the direction $\hat{\omega}$, arriving at the Sun at a time t, the output in an equal-arm space-based interferometric detector such as LISA, TianQin and Taiji with a single round-trip of light travel is

$$s(t) = \sum_A F^A h_A(t) e^{i\phi_D(t)}, \tag{5}$$

$$\phi_D(t) = \frac{2\pi f R}{c}\sin\theta\cos\left(\frac{2\pi t}{P} + \phi_\alpha - \phi\right), \tag{6}$$

$$F^A = \sum_{i,j} D^{ij} e^A_{ij}, \tag{7}$$

where F^A is the pattern function for the polarization mode A, $\phi_D(t)$ is the Doppler phase, ϕ_α is the ecliptic longitude of the detector α at $t = 0$, the rotational period P is 1 yr and the radius R of the orbit is 1 A.U. The detector tensor D^{ij} is

$$D^{ij} = \frac{1}{2}[\hat{u}^i\hat{u}^j T(f, \hat{u}\cdot\hat{\omega}) - \hat{v}^i\hat{v}^j T(f, \hat{v}\cdot\hat{\omega})], \tag{8}$$

where $\hat{u}$ and $\hat{v}$ are the unit vectors along the arms of the detector. The detailed orbit equations are presented in Appendix A. Additionally, $T(f, \hat{u}\cdot\hat{\omega})$ is [70,71]

$$\begin{aligned}
T(f, x) = \frac{1}{2}\Bigg\{&\mathrm{sinc}\left[\frac{f(1-x)}{2f^*}\right]\exp\left[\frac{f(3+x)}{2if^*}\right]\\
&+ \mathrm{sinc}\left[\frac{f(1+x)}{2f^*}\right]\exp\left[\frac{f(1+x)}{2if^*}\right]\Bigg\},
\end{aligned} \tag{9}$$

where $\mathrm{sinc}(x) = \sin x/x$, $f^* = c/(2\pi L)$ is the transfer frequency of the detector, c is the speed of light and L is the arm length of the detector. Note that in the long-wavelength approximation $f \ll f^*$, we have $T(f, \hat{u}\cdot\hat{\omega}) \to 1$ in Eq. (9). The triangle configuration of the proposed space-based GW detector such as LISA, TianQin, and Taiji

can be regarded as two L-shaped detectors effectively. In this paper we only consider the Michelson interferometer consisting of two equal arms with the unit vectors $\hat{u}$ and $\hat{v}$ for simplicity. To significantly reduce the laser frequency noise due to unequal arm lengths, time-delay interferometry (TDI) [72,73] is needed. We discuss the GW response for the TDI Michelson variable X in Appendix B. The averaged response function $|F^A|^2$ including different TDI combinations for different polarization mode A was discussed in [74–80].

III. METHODOLOGY

Now we consider the strain output $d(t)$ produced by a monochromatic GW for a space-based GW detector in the heliocentric coordinate system. A monochromatic GW assumed to be emitted from a source with the sky location $-\hat{\omega}(\theta,\phi)$, arrives at the Sun at the time t. If only the tensor-polarization modes are present, we have

$$d_w(t) = F_w^+(\hat{\omega},f,t)h_+(t)e^{i\phi_D(t)} + F_w^\times(\hat{\omega},f,t)h_\times(t)e^{i\phi_D(t)} + n_w(t), \tag{10}$$

where F_w^+ and $F_w^\times$ are the noise-weighted beam pattern functions and $n_w(t)$ is the whitened noise. The noise-weighted beam pattern functions and noise-weighted data are [81]

$$F_w^A = \frac{F^A}{\sqrt{S_n(f)}}, \quad d_w = \frac{d}{\sqrt{S_n(f)}}. \tag{11}$$

In the following we always use the noise-weighted beam pattern functions and noise-weighted data, so we ignore the label w for simplicity. For space-based interferometers, the noise power spectral density $S_n(f)$ is [64,65,82,83]

$$S_n(f) = \frac{S_x}{L^2} + \frac{2S_a(1+\cos^2(f/f^*))}{(2\pi f)^4 L^2}\left(1+\left(\frac{0.4\,\mathrm{mHz}}{f}\right)^2\right). \tag{12}$$

For LISA, the acceleration noise is $\sqrt{S_a} = 3\times 10^{-15}\,\mathrm{m\,s^{-2}/Hz^{1/2}}$, the displacement noise is $\sqrt{S_x} = 15\,\mathrm{pm/Hz^{1/2}}$, the arm length is $L = 2.5\times 10^6$ km, and its transfer frequency is $f^* = 0.02$ Hz [64]. Similarly, for TianQin $\sqrt{S_a} = 10^{-15}\ \mathrm{m\,s^{-2}/Hz^{1/2}}$, $\sqrt{S_x} = 1\ \mathrm{pm/Hz^{1/2}}$, $L = \sqrt{3}\times 10^5$ km, and $f^* = 0.28$ Hz [65]. For Taiji $\sqrt{S_a} = 3\times 10^{-15}\ \mathrm{m\,s^{-2}/Hz^{1/2}}$, $\sqrt{S_x} = 8\ \mathrm{pm/Hz^{1/2}}$, $L = 3\times 10^6$ km, and $f^* = 0.016$ Hz [84].

Taking the source J0806.3 + 1527 located at ($\theta = 94.7°$, $\phi = 120.5°$) as an example, we simulate the strain output in a space-based GW detector. In GR the quadrupole formula provides the lowest-order post-Newtonian GW waveform for a binary system as[1]

$$h_+ = \mathcal{A}[1+\cos^2(\iota)]\exp(2\pi i f_0 t + i\phi_0), \quad h_\times = 2i\mathcal{A}\cos(\iota)\exp(2\pi i f_0 t + i\phi_0), \tag{13}$$

where $\mathcal{A} = 2(G\mathcal{M}/c^2)^{5/3}(\pi f/c)^{2/3}/D_L$ is the GW overall amplitude, $\mathcal{M} = 0.3\ M_\odot$ (we take the component masses 0.5 $M_\odot$ and 0.25 $M_\odot$) is the chirp mass, $D_L = 0.5$ kpc is the luminosity distance, $\iota = \pi/6$ is the inclination angle between the line of sight and the binary orbital axis, ϕ_0 is the initial GW phase at the start of observation, and $f_0 = 6.22$ mHz is the emitted GW frequency of the source J0806.3 + 1527 [85–89]. The signal in Eq. (10) can be rewritten in another form

$$d(t) = \bar{h}_+ F^+(\hat{\omega},f_0,t)e^{2\pi i f_0 t + i\phi_D(t)} + \bar{h}_\times F^\times(\hat{\omega},f_0,t)e^{2\pi i f_0 t + i\phi_D(t)} + n(t), \tag{14}$$

where

$$\bar{h}_+ = \mathcal{A}[1+\cos^2(\iota)]\exp(i\phi_0), \quad \bar{h}_\times = 2i\mathcal{A}\cos(\iota)\exp(i\phi_0).$$

We denote N number of the observational data $d[k] = d(t_k)$ at discrete times in a more compact matrix form

$$\mathbf{d}[k] = \mathbf{F}\mathbf{h}[k] + \mathbf{n}[k], \tag{15}$$

where

$$\mathbf{d} = \begin{pmatrix} d[0] \\ \vdots \\ d[k] \end{pmatrix}, \quad \mathbf{h} = \begin{pmatrix} \bar{h}_+ \\ \bar{h}_\times \end{pmatrix}, \quad \mathbf{n} = \begin{pmatrix} n[0] \\ \vdots \\ n[k] \end{pmatrix}, \tag{16}$$

$$\mathbf{F} = (\,\mathbf{F}^+ \quad \mathbf{F}^\times\,) = \begin{pmatrix} F^+(t_0)e^{2\pi i f_0 t_0 + i\phi_D(t_0)} & F^\times(t_0)e^{2\pi i f_0 t_0 + i\phi_D(t_0)} \\ \vdots & \vdots \\ F^+(t_n)e^{2\pi i f_0 t_n + i\phi_D(t_n)} & F^\times(t_n)e^{2\pi i f_0 t_n + i\phi_D(t_n)} \end{pmatrix}, \tag{17}$$

$k = 0, 1, 2, \ldots, N-1$ labels the data observed by the detector at the time $t_k = k * \Delta t$ and $1/\Delta t$ is the sampling rate. The GW signal $\mathbf{s} = \mathbf{F}\mathbf{h}$ spanned by $\mathbf{F}^+$ and $\mathbf{F}^\times$ can be viewed as being in a subspace of the space of detector

[1] In Eq. (13), f_0 should be the observed frequency which is related with the emitted frequency f_e as $f_0 = f_e/(1+z)$ and the chirp mass $\mathcal{M}$ in the source frame should be $(1+z)\mathcal{M}$ in the detector frame.

output. We can construct the *null projector* $\mathbf{P}_{\rm null}(\hat{\omega}, f_0)$ [90] to project away the signal if the projector is constructed with the source's sky location and GW frequency [34]. The null projector is given by

$$\mathbf{P}_{\rm null} = \mathbf{I} - \mathbf{F}(\mathbf{F}^\dagger\mathbf{F})^{-1}\mathbf{F}^\dagger, \tag{18}$$

where † denotes the Hermitian conjugation. Applying the null projector on the strain data $\mathbf{d}$ in Eq. (15), we obtain

$$\begin{aligned}\mathbf{z} &= \mathbf{P}_{\rm null}(\hat{\omega}, f_0)\mathbf{d} \\ &= \mathbf{P}_{\rm null}(\hat{\omega}, f_0)\mathbf{F}(\hat{\omega}, f_0)\mathbf{h} + \mathbf{P}_{\rm null}(\hat{\omega}, f_0)\mathbf{n} \\ &= \mathbf{P}_{\rm null}(\hat{\omega}, f_0)\mathbf{n},\end{aligned} \tag{19}$$

where $\mathbf{z}$ is the *null stream* which only consists of the noise living in a subspace that is orthogonal to the one spanned by $\mathbf{F}^+$ and $\mathbf{F}^\times$.

To consider the effect of polarization modes other than tensor modes, we parameterize the extra polarization modes in the tensor-scalar, tensor-vector and tensor-vector-scalar models with different strengths of nontensorial components. Following [91], we take the waveforms of the extra polarization modes in the tensor-scalar model as

$$\begin{aligned}h_b &= B\mathcal{A}\sin^2(\iota)\exp(2\pi i f_0 t + i\phi_0), \\ h_l &= \sqrt{2}B\mathcal{A}\sin^2(\iota)\exp(2\pi i f_0 t + i\phi_0),\end{aligned} \tag{20}$$

where B denotes the relative amplitude of the scalar modes to the tensor modes. The waveforms of the extra polarization modes in the tensor-vector model are [91]

$$\begin{aligned}h_x &= B\mathcal{A}\sin(2\iota)\exp(2\pi i f_0 t + i\phi_0), \\ h_y &= 2B\mathcal{A}\sin(\iota)\exp(2\pi i f_0 t + i\phi_0),\end{aligned} \tag{21}$$

where B denotes the relative amplitude of the vector modes to the tensor modes. The waveforms of the extra polarization modes in the tensor-vector-scalar model are [91]

$$\begin{aligned}h_x &= B\mathcal{A}\sin(2\iota)\exp(2\pi i f_0 t + i\phi_0), \\ h_y &= 2B\mathcal{A}\sin(\iota)\exp(2\pi i f_0 t + i\phi_0), \\ h_b &= B\mathcal{A}\sin^2(\iota)\exp(2\pi i f_0 t + i\phi_0), \\ h_l &= \sqrt{2}B\mathcal{A}\sin^2(\iota)\exp(2\pi i f_0 t + i\phi_0),\end{aligned} \tag{22}$$

where B denotes the relative amplitude of the nontensorial modes to the tensor modes. Including the polarization contents beyond tensor polarizations, the signal can be written in the form

$$d(t) = \sum_A \bar{h}_A F^A(\hat{\omega}, f_0, t) e^{2\pi i f_0 t + i\phi_D(t)} + n(t). \tag{23}$$

The observational data matrix (15) becomes

$$\mathbf{d}[k] = \mathbf{F}^t(\hat{\omega}, f_0)\mathbf{h}_t[k] + \mathbf{F}^e(\hat{\omega}, f_0)\mathbf{h}_e[k] + \mathbf{n}[k], \tag{24}$$

where the superscript t means summing over $+$ and $\times$, while the superscript e means summing over whatever additional polarizations present. For example, the observational data matrix (15) in the tensor-scalar model becomes

$$\begin{aligned}\mathbf{d}[k] = {} & \mathbf{F}^+(\hat{\omega}, f_0)\bar{h}_+[k] + \mathbf{F}^\times(\hat{\omega}, f_0)\bar{h}_\times[k] \\ & + \mathbf{F}^b(\hat{\omega}, f_0)\bar{h}_b[k] + \mathbf{F}^l(\hat{\omega}, f_0)\bar{h}_l[k] + \mathbf{n}[k].\end{aligned} \tag{25}$$

The null stream obtained from the null projector with pure-tensor beam pattern matrix is given by

$$\begin{aligned}\mathbf{z}[k] &= \mathbf{P}_{\rm null}(\hat{\omega}, f_0)\mathbf{d}[k] \\ &= \mathbf{P}_{\rm null}(\hat{\omega}, f_0)\mathbf{n}[k] + \mathbf{P}_{\rm null}\mathbf{F}^e(\hat{\omega}, f_0)\mathbf{h}_e[k].\end{aligned} \tag{26}$$

The last term signifies the presence of extra polarizations other than tensor modes. If there are additional polarization modes in GWs, then the data $\tilde{\mathbf{z}}[k]$ which is the discrete Fourier transformation of $\mathbf{z}[k]$ [90] has a discrete component at f_0 in the frequency domain.

A. Simulation result

For the reference source J0806.3 + 1527 and the total observation time of one year, we choose the sampling rate as 0.02 Hz, so $N = 365 \times 24 \times 3600 \times 0.02 = 630720$. We inject a set of mock waveforms with $B = \{0, 0.4, 0.8\}$ in addition to simulated signals from GR. The results for the tensor-scalar, tensor-vector and tensor-vector-scalar models with LISA, TianQin, and Taiji are shown in Figs. 1, 2, and 3, respectively. The figures with $B = 0$ show that this method can eliminate the tensor polarization if there is no extra polarization mode. From figures with $B = \{0.4, 0.8\}$ we see that extra polarization modes in the tensor-vector and tensor-vector-scalar models can be detected by LISA and Taiji. For the tensor-scalar model, extra polarization modes with $B = 0.8$ can be detected by Taiji. The reason is that extra polarization signals should be loud enough for the detection. The figures also show that extra polarization components with larger relative amplitude B can be detected more easily. From Fig. 2, we see that it is impossible to detect any extra polarization with TianQin for any model and any value of B using this method. To quantify the detection of extra polarization, we use the signal-to-noise (SNR) ρ [92],

$$\rho^2 = \int_0^\infty df \frac{4|\tilde{h}(f)|^2}{S_n(f)} = \frac{4|\tilde{\mathbf{z}}|^2_{f=f_0}}{S_{\tilde{\mathbf{z}}}}, \tag{27}$$

where $|\tilde{\mathbf{z}}|_{f=f_0}$ represents the amplitude of $\tilde{\mathbf{z}}$ at frequency f_0 and $S_{\tilde{\mathbf{z}}}$ represents the noise power spectrum of $\tilde{\mathbf{z}}$, shown in Fig. 4. With $B = \{0.4, 0.8\}$ and one-year observation time, we get $\{\rho < 7, \rho < 7\}$ for LISA and $\{\rho < 7, \rho = 11.6\}$ for Taiji in the tensor-scalar model, $\rho = \{57.4, 113.3\}$ for LISA and $\rho = \{77.5, 157.1\}$ for Taiji in the tensor-vector model, $\rho = \{57.3, 113.9\}$ for LISA and $\rho = \{77.6, 154.9\}$ for Taiji

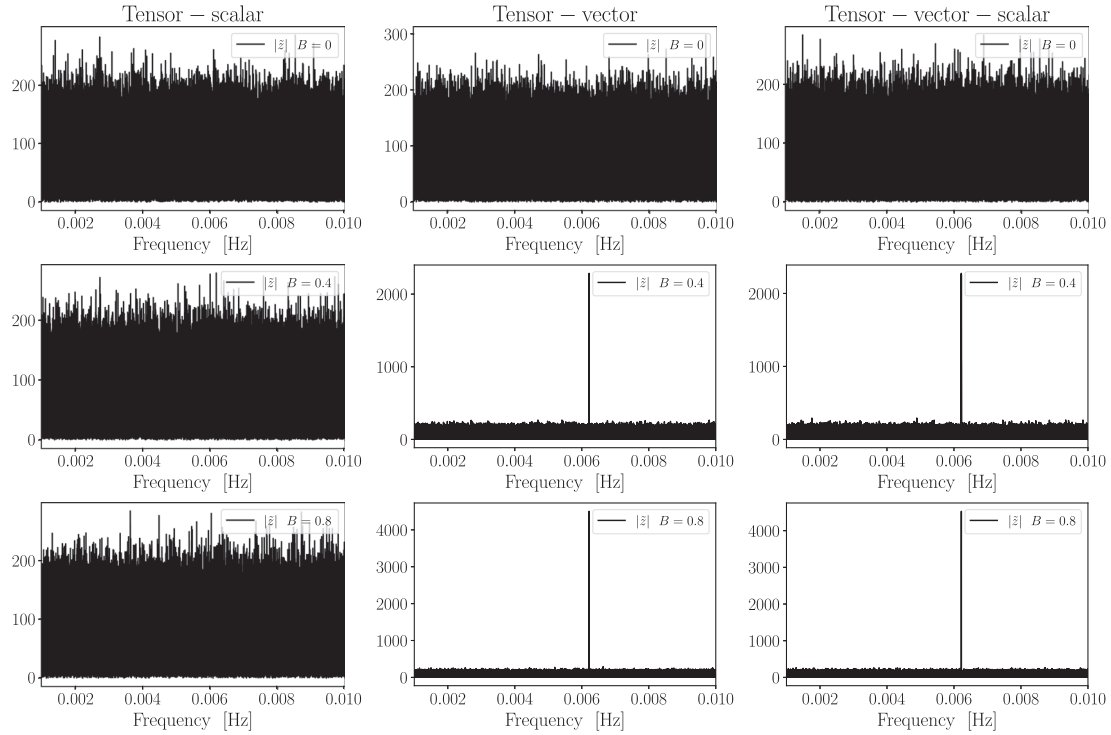

FIG. 1. The results of the null stream $|\tilde{z}|$ for the source J0806.3 + 1527 with LISA in the tensor-scalar (left panel), tensor-vector (middle panel), and tensor-vector-scalar (right panel) models.

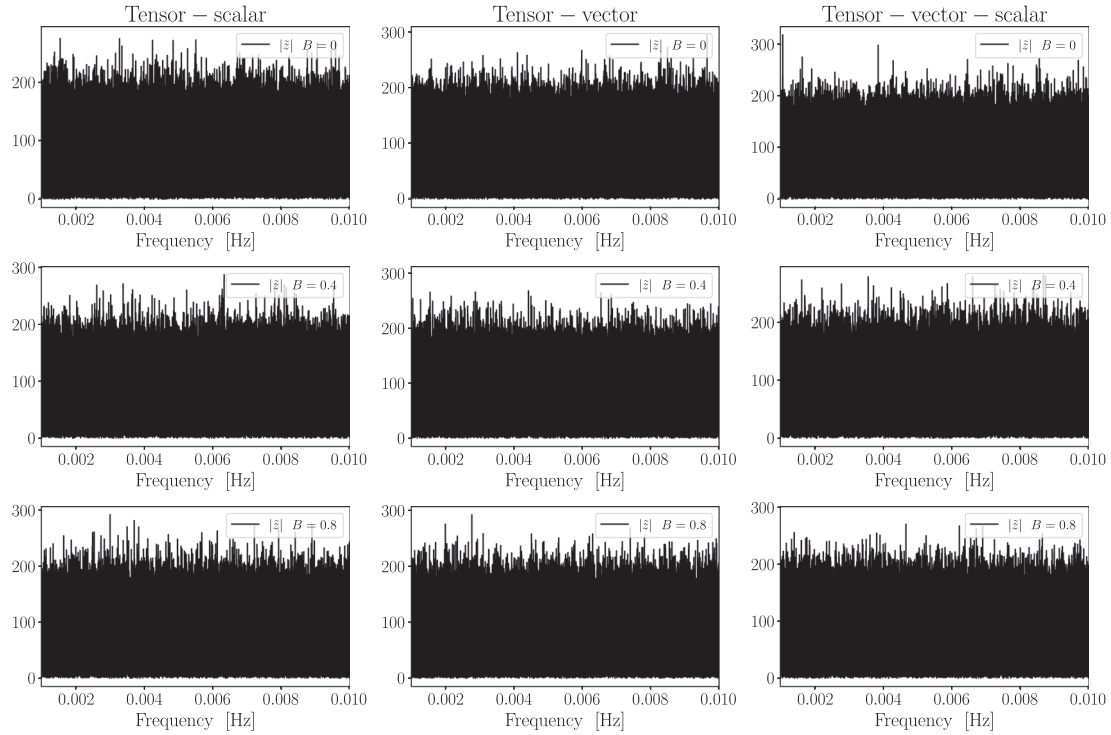

FIG. 2. The results of the null stream $|\tilde{z}|$ for the source J0806.3 + 1527 with TianQin in the tensor-scalar (left panel), tensor-vector (middle panel), and tensor-vector-scalar (right panel) models.

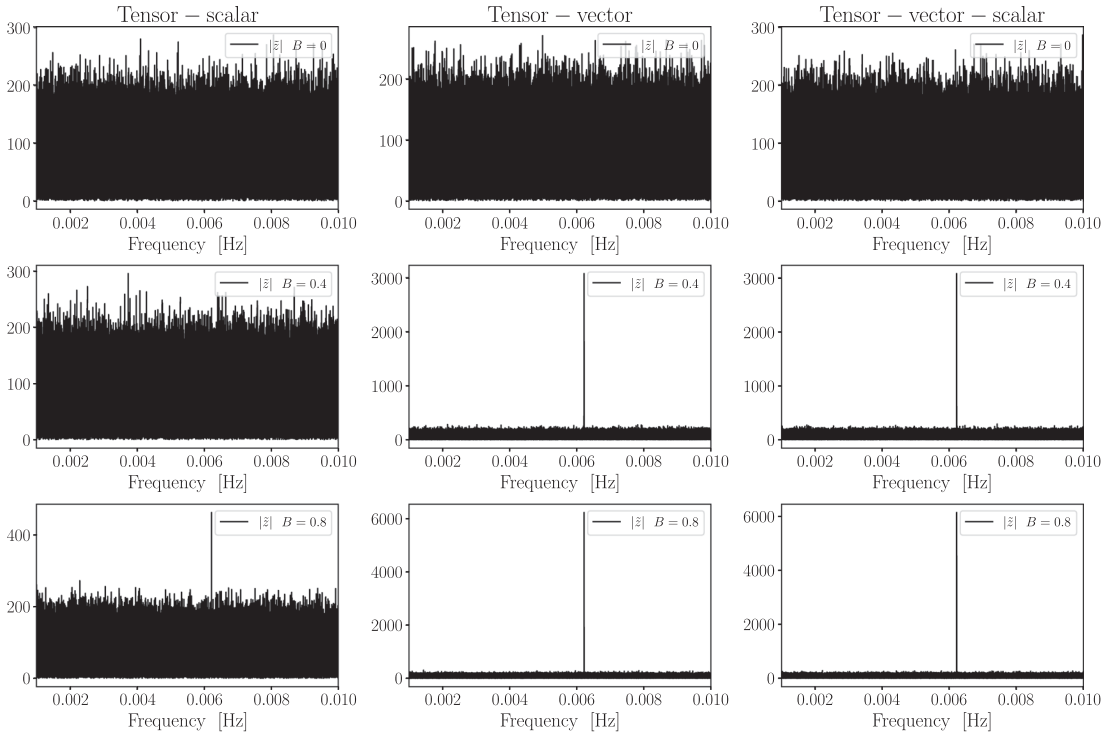

FIG. 3. The results of the null stream $|\tilde{z}|$ for the source J0806.3 + 1527 with Taiji in the tensor-scalar (left panel), tensor-vector (middle panel), and tensor-vector-scalar (right panel) models.

in the tensor-vector-scalar model. For TianQin we get $\rho < 7$ in the tensor-scalar, tensor-vector and tensor-vector-scalar models with $B = \{0.4, 0.8\}$ and a one year observation time. To get $\rho > 7$ with one year observation time, we find LISA requires $B > 3.3$, $B > 5 \times 10^{-2}$, and $B > 5 \times 10^{-2}$ in the tensor-scalar, tensor-vector and tensor-vector-scalar models, respectively; Taiji requires $B > 0.49$, $B > 3.8 \times 10^{-2}$, and $B > 3.8 \times 10^{-2}$ in the tensor-scalar, tensor-vector and tensor-vector-scalar models, respectively. In order to avoid the limitation of the conclusion because it was drawn from one particular rather than a global representation of the performance of the detector, we choose several representative locations for the J0806.3 + 1527-like source and the results with LISA and Taiji are shown in Table I. Except the location (θ, ϕ), all other parameters for the sources are the same as J0806.3 + 1527. For all the sources and models, we get $\rho < 7$ with TianQin. These results show that the conclusion that the method can be used by LISA and Taiji to detect extra polarizations is robust. Due to the orbital motion of the detector in space, along its trajectory, a detector like LISA and Taiji can be effectively regarded as a set of virtual detectors at different positions and therefore form a network with N number of virtual detectors to measure the polarization contents of monochromatic GW signals. However, TianQin always points to the reference source J0806.3 + 1527 without changing the orientation of its detector plane, so TianQin cannot use this method to detect the polarization contents of monochromatic GWs.

Accurately localizing GW sources is very important for measuring extra polarizations. To show this point, we construct the null projector with a sky position different from the source's true location to project the signal and the results are shown in Fig. 5. From Fig. 5, we see that when the sky position for constructing the null projector is away from the source's true location, the null projector can not eliminate the tensor polarizations. Therefore, we can not distinguish extra polarizations from tensor polarizations if the sky location is not accurately known. Fortunately, for space-based GW detectors, the accuracy of sky localizations is enough for constructing the null projector.

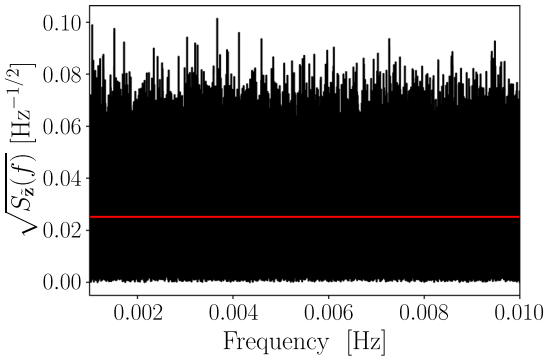

FIG. 4. The noise power spectrum $S_{\tilde{\mathbf{z}}}(f)$. The red line is the average value of $S_{\tilde{\mathbf{z}}}$.

TABLE I. SNRs in LISA and Taiji for the tensor-scalar, tensor-vector, and tensor-vector-scalar models with $B = \{0.4, 0.8\}$. In addition to the locations (θ, ϕ) listed in the table, the other parameters are ($\mathcal{M} = 0.3\ M_\odot$, $D_L = 0.5$ kpc, $\iota = \pi/6$, $\phi_0 = 0$, $f_0 = 6.22$ mHz).

Location	Tensor-scalar model		Tensor-vector model		Tensor-vector-scalar model	
(θ, ϕ)	LISA	Taiji	LISA	Taiji	LISA	Taiji
(0.3, 5.0)	$\{< 7, 8.1\}$	$\{8.4, 13.5\}$	$\{64.4, 126.7\}$	$\{93.0, 188.3\}$	$\{62.8, 125.3\}$	$\{98.2, 191.4\}$
(0.3, 1.0)	$\{< 7, < 7\}$	$\{8.3, 15.6\}$	$\{57.3, 105.4\}$	$\{133.3, 263.0\}$	$\{54.4, 107.5\}$	$\{126.0, 257.4\}$
$(-0.3, 5.0)$	$\{< 7, 9.4\}$	$\{7.4, 11.7\}$	$\{64.0, 125.0\}$	$\{90.7, 181.7\}$	$\{68.6, 132.3\}$	$\{87.4, 174.1\}$
$(-0.3, 1.0)$	$\{< 7, 7.6\}$	$\{< 7, 18.0\}$	$\{55.7, 111.7\}$	$\{131.7, 265.1\}$	$\{51.6, 109.5\}$	$\{136.8, 274.2\}$
(1.0, 5.0)	$\{< 7, < 7\}$	$\{< 7, 9.9\}$	$\{49.1, 94.1\}$	$\{79.7, 159.5\}$	$\{47.0, 95.2\}$	$\{81.4, 166.4\}$

B. Improved methodology

The original methodology is based on the assumption that detectors like LISA and Taiji can be effectively regarded as a set of virtual detectors at different position and therefore, form a network with N number of virtual detectors to measure the polarization contents of monochromatic GW signals. However, it is well known that instead of N number of detectors, three detectors with different orientations are enough to discriminate extra polarization mode from the tensor modes. Based on this fact, we split the data of one year observation into three identical lengthy segments with four months data in each and regard them as three independent detectors' data. This improved method decreases the number of virtual detectors but increases the effective observation time for each detector. It reduces computational memory and time because we only need to handle a 3-dimensional matrix rather than an N-dimensional matrix each time. The observation time T for each virtual detector becomes four months, and the three data segments are

$$s_0(t) = (F^+(t)h_+(t) + F^\times(t)h_\times(t))e^{i\phi_D(t)}, \quad (28)$$

$$s_1(t) = F^+(t+T)h_+(t+T)e^{i\phi_D(t+T)} + F^\times(t+T)h_\times(t+T)e^{i\phi_D(t+T)}, \quad (29)$$

$$s_2(t) = F^+(t+2T)h_+(t+2T)e^{i\phi_D(t+2T)} + F^\times(t+2T)h_\times(t+2T)e^{i\phi_D(t+2T)}. \quad (30)$$

We rewrite the three detectors' observation data in matrix form

$$\mathbf{d}(t) = \mathbf{F}(t)\mathbf{h} + \mathbf{n}(t), \quad (31)$$

where

$$\mathbf{d}(t) = \begin{pmatrix} d_0(t) \\ d_1(t) \\ d_2(t) \end{pmatrix}, \quad \mathbf{h} = \begin{pmatrix} \bar{h}_+ \\ \bar{h}_\times \end{pmatrix}, \quad \mathbf{n}(t) = \begin{pmatrix} n(t) \\ n(t+T) \\ n(t+2T) \end{pmatrix},$$

and

$$\mathbf{F}(t) = \begin{pmatrix} F^+(t)e^{2\pi i f t + i\phi_D(t)} & F^\times(t)e^{2\pi i f_0 t + i\phi_D(t)} \\ F^+(t+T)e^{2\pi i f_0(t+T) + i\phi_D(t+T)} & F^\times(t+T)e^{2\pi i f_0(t+T) + i\phi_D(t+T)} \\ F^+(t+2T)e^{2\pi i f_0(t+2T) + i\phi_D(t+2T)} & F^\times(t+2T)e^{2\pi i f_0(t+2T) + i\phi_D(t+2T)} \end{pmatrix}. \quad (32)$$

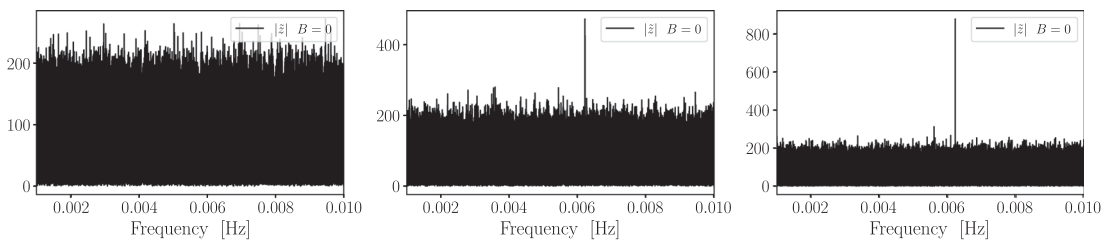

FIG. 5. The results of the null stream $|\tilde{z}|$ with the null projector constructed by a sky position different from the true source for LISA. The sky position is at $(\theta = 94.7° + 0.06°, \phi = 120.5° + 0.06°)$ in the left panel, $(\theta = 94.7° + 0.3°, \phi = 120.5° + 0.3°)$ in the middle panel, and $(\theta = 94.7° + 0.6°, \phi = 120.5° + 0.6°)$ in the right panel.

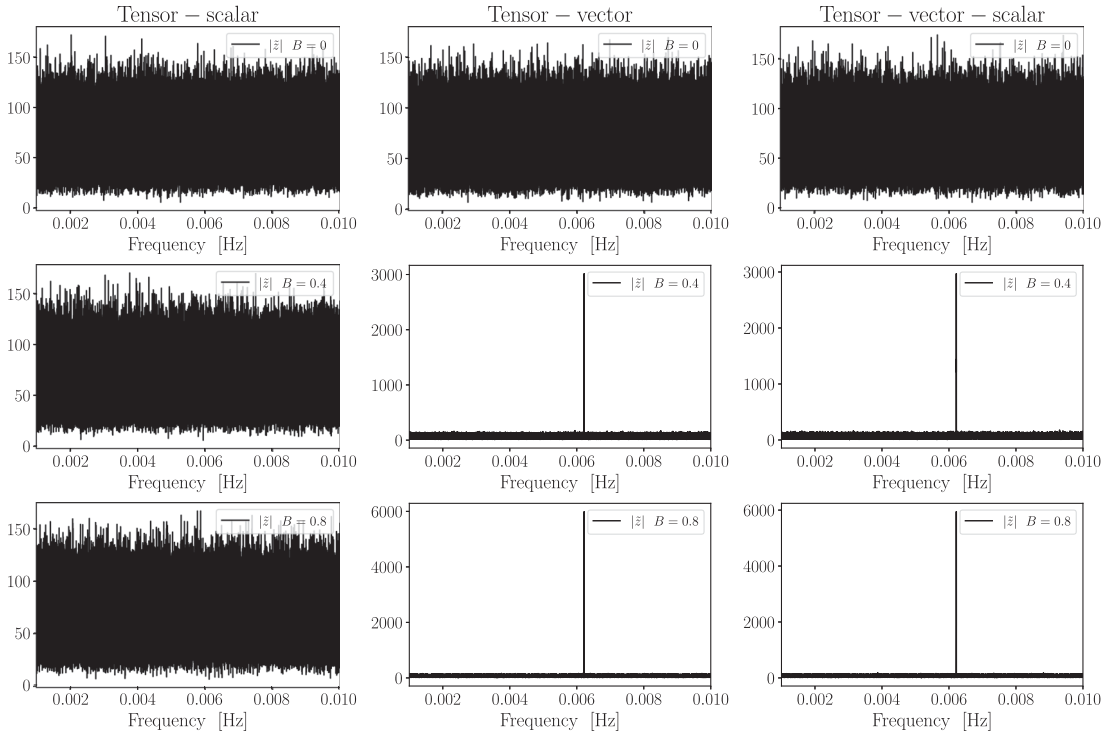

FIG. 6. The results of the null stream $|\tilde{z}| = \sqrt{|\tilde{z}_0|^2 + |\tilde{z}_1|^2 + |\tilde{z}_2|^2}$ for the source J0806.3 + 1527 with LISA in the tensor-scalar (left panel), tensor-vector (middle panel), and tensor-vector-scalar (right panel) models.

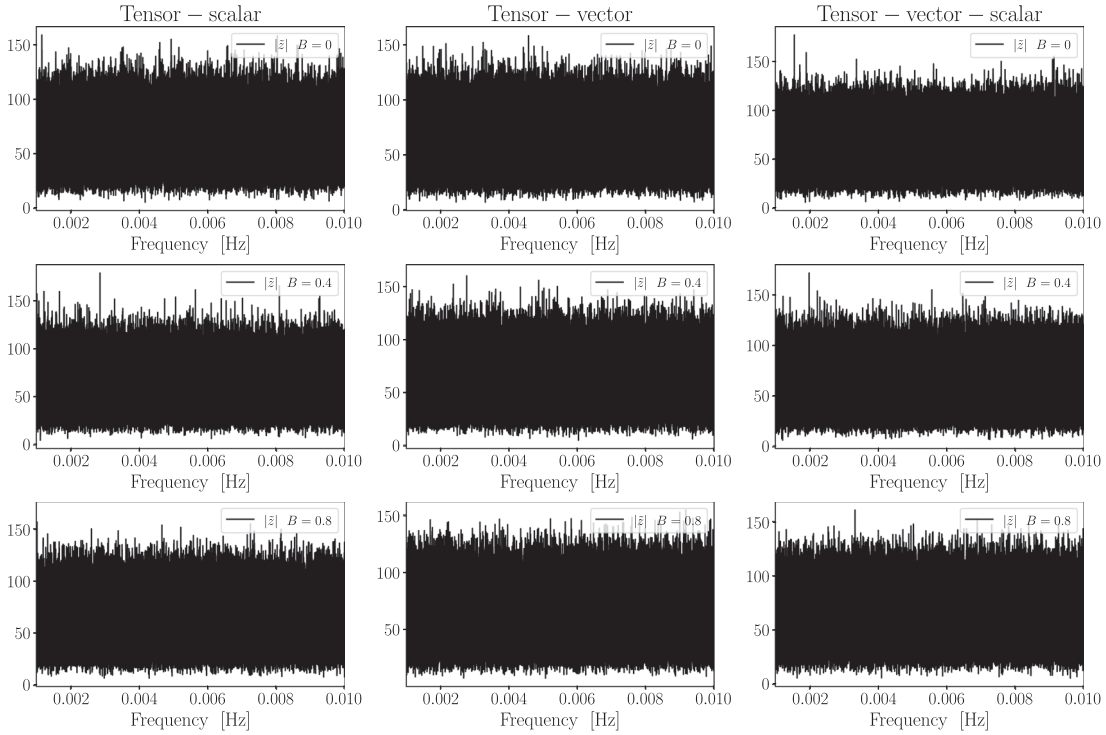

FIG. 7. The results of the null stream $|\tilde{z}| = \sqrt{|\tilde{z}_0|^2 + |\tilde{z}_1|^2 + |\tilde{z}_2|^2}$ for the source J0806.3 + 1527 with TianQin in the tensor-scalar (left panel), tensor-vector (middle panel), and tensor-vector-scalar (right panel) models.

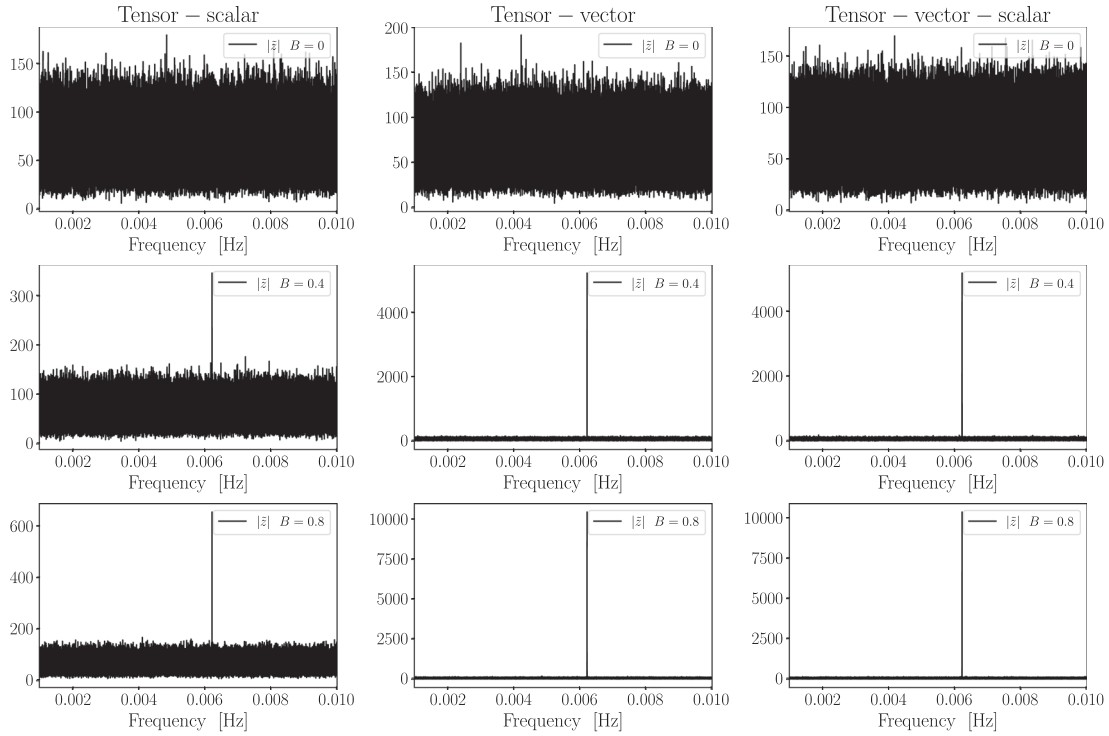

FIG. 8. The results of the null stream $|\tilde{z}| = \sqrt{|\tilde{z}_0|^2 + |\tilde{z}_1|^2 + |\tilde{z}_2|^2}$ for the source J0806.3 + 1527 with Taiji in the tensor-scalar (left panel), tensor-vector (middle panel), and tensor-vector-scalar (right panel) models.

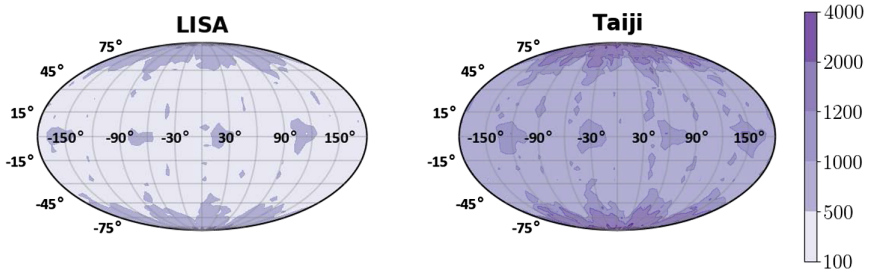

FIG. 9. The sky map of SNRs in LISA (left panel) and Taiji (right panel) for the tensor-vector-scalar model with $B = 0.8$. The parameters for the sources are $\mathcal{M} = 0.3\ M_\odot$, $D_L = 0.5$ kpc, $\iota = \pi/6$, $\phi_0 = 0$, and $f_0 = 6.22$ mHz.

The signal can be seen as the data observed at a given time t by three different detectors at the same time. Within the observation period of four months, there are many observation points. For any given time, we get

$$\begin{aligned}\mathbf{z}(t) &= \mathbf{P}_{\text{null}}(t)\mathbf{d}(t) \\ &= \mathbf{P}_{\text{null}}\mathbf{n} + \mathbf{P}_{\text{null}}\mathbf{F}^e(t)\mathbf{h}_e,\end{aligned} \tag{33}$$

where $\mathbf{z}(t) = (z_0(t), z_1(t), z_2(t))^T$. For three virtual detectors, the total SNR is

$$\rho^2 = \rho_{\tilde{z}_0}^2 + \rho_{\tilde{z}_1}^2 + \rho_{\tilde{z}_2}^2. \tag{34}$$

We apply the method (33) to detect extra polarizations in the tensor-scalar, tensor-vector, and tensor-vector-scalar models. For the reference source J0806.3 + 1527 and the total observation time of one year, we choose the sampling rate as 0.02 Hz. The results are shown in Figs. 6, 7, and 8 for LISA, TianQin, and Taiji respectively. For LISA and $B = \{0.4, 0.8\}$, we get $\rho = \{148, 294\}$ in the tensor-vector model and $\rho = \{146, 292\}$ in the tensor-vector-scalar model. For Taiji and $B = \{0.4, 0.8\}$, we get $\rho = \{19, 34\}$ in the tensor-scalar model, $\rho = \{258, 517\}$ in the tensor-vector model and $\rho = \{256, 513\}$ in the tensor-vector-scalar model. To get $\rho > 7$ with a one year observation time, we find that LISA requires $B > 3.1$, $B > 1.9 \times 10^{-2}$, and $B > 1.9 \times 10^{-2}$ in the tensor-scalar, tensor-vector, and tensor-vector-scalar models, respectively; Taiji requires $B > 0.2$, $B > 1.5 \times 10^{-2}$, and $B > 1.5 \times 10^{-2}$ in the tensor-scalar, tensor-vector, and tensor-vector-scalar models, respectively.

We also simulate 2500 sources uniformly distributed in the sky with $-\pi/2 < \theta < \pi/2$ and $-\pi < \phi < \pi$. Except for the locations, the other parameters of the sources are the same as for the source J0806.3 + 1527. Simulating the data in the detector with the waveforms (22) for the tensor-

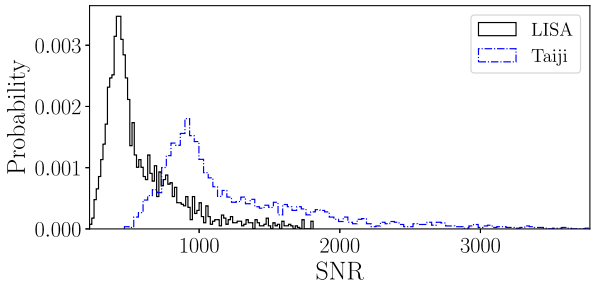

FIG. 10. Histograms of SNRs in LISA and Taiji for the tensor-vector-scalar model with $B = 0.8$.

vector-scalar model with $B = 0.8$, we then apply method (33) to calculate the total SNR. The sky map and the histogram of the SNR for Taiji and LISA are shown in Figs. 9 and 10, respectively. The mean value of SNR is 571 with LISA and 1215 with Taiji for the tensor-vector-scalar model with $B = 0.8$. The results show that LISA and Taiji can detect extra polarization modes with relative large B for sources from all directions.

IV. CONCLUSION

We introduce a concrete data analysis pipeline to test extra polarization modes of monochromatic GWs for space-based GW detectors. This null-stream method is applicable to LISA and Taiji because of their changing orientation of the detector plane. We first take the single detector as N virtual detectors by dividing the observational data into N segments and use the source J0806.3 + 1527 as an example to simulate GW signals in the detector. For a one year observation with the signal-to-noise of $\rho > 7$, we find that LISA can detect extra polarizations with the relative amplitude $B > 3.3$, $B > 5 \times 10^{-2}$, and $B > 5 \times 10^{-2}$ in the tensor-scalar, tensor-vector, and tensor-vector-scalar models, respectively; Taiji can detect extra polarizations with $B > 0.49$, $B > 3.8 \times 10^{-2}$, and $B > 3.8 \times 10^{-2}$ in the tensor-scalar, tensor-vector, and tensor-vector-scalar models, respectively. We also analyzed the impact of the number of virtual detectors on the detection of extra polarization modes and we find that three virtual detectors with more observational time for each virtual detector can better detect extra polarization modes.

We then divide the one-year observational data into three identical segments to effectively form three virtual detectors. With this method, the computational cost is much less. For $\rho > 7$, LISA can detect extra polarizations with the relative amplitude $B > 3.1$, $B > 1.9 \times 10^{-2}$, and $B > 1.9 \times 10^{-2}$ in the tensor-scalar, tensor-vector, and tensor-vector-scalar models, respectively, and Taiji can detect extra polarizations with $B > 0.2$, $B > 1.5 \times 10^{-2}$, and $B > 1.5 \times 10^{-2}$ in the tensor-scalar, tensor-vector, and tensor-vector-scalar models, respectively. The results show that the ability of detecting extra polarizations is almost the same in the tensor-vector and tensor-vector-scalar models, but the method is less effective in detecting extra scalar modes. To discuss the dependence on the source location, we simulate 2500 signals from the tensor-vector-scalar model with $B = 0.8$ by distributing the sources uniformly in the sky, the mean value of SNR is 571 for LISA and it is 1215 for Taiji. If the sky location of the source is not accurately known, then the method can not be applied to measure the polarizations. Therefore, this method can not be used to detect the polarization modes of stochastic background GWs. To detect the polarization modes of stochastic GW backgrounds, we need to combine multiple correlation signals as discussed in [38]. Similar to the idea of a virtual detector network considered in this paper, the cross-correlation measured at different times can be regarded as an independent set of signals with different location and separation, these signals form a virtual network and help to improve the detection sensitivity [38]. By combining the technique of cross-correlation with our method, space-based GW detectors such LISA, TianQin, and Taiji can detect polarization modes of stochastic GW backgrounds.

In conclusion, the method of the null stream can be applied to LISA and Taiji to detect extra polarization modes of monochromatic GWs.

ACKNOWLEDGMENTS

This work is supported by the National Natural Science Foundation of China under Grant No. 11875136 and the Major Program of the National Natural Science Foundation of China under Grant No. 11690021. D. L. is supported by the China Postdoctoral Science Foundation under Grant No. 2021TQ0018 and the National Natural Science Foundation of China under Grant No. 12147120.

APPENDIX A: DETECTOR'S ORBITS

1. TianQin's orbits

In the heliocentric coordinate system, the normal vector of TianQin's detector plane points to the direction of RX J0806.3 + 1527 with the latitude $\beta = 94.7°$ and the longitude $\alpha = 120.5°$. The orbits of the unit vectors of detector arms (two arms only) for TianQin are [83]

$$\hat{u}_x = \cos(\omega_s t)\cos(\alpha)\cos(\beta) - \sin(\omega_s t)\sin(\alpha),$$
$$\hat{u}_y = \cos(\alpha)\sin(\omega_s t) + \cos(\omega_s t)\cos(\beta)\sin(\alpha),$$
$$\hat{u}_z = -\cos(\omega_s t)\sin(\beta),$$
$$\hat{v}_x = \cos\left(\omega_s t + \frac{\pi}{3}\right)\cos(\alpha)\cos(\beta) - \sin\left(\omega_s t + \frac{\pi}{3}\right)\sin(\alpha),$$
$$\hat{v}_y = \cos(\alpha)\sin\left(\omega_s t + \frac{\pi}{3}\right) + \cos\left(\omega_s t + \frac{\pi}{3}\right)\cos(\beta)\sin(\alpha),$$
$$\hat{v}_z = -\cos\left(\omega_s t + \frac{\pi}{3}\right)\sin(\beta),$$

where the rotation frequency $\omega_s = 2\pi/(3.65 \text{ days})$.

2. The orbits for LISA and Taiji

In the heliocentric coordinate system, the detector's center-of-mass follows the trajectory

$$\bar{\theta}(t) = \pi/2, \qquad \bar{\phi}(t) = 2\pi t/T + \phi_\alpha, \tag{A1}$$

where T equals one year and ϕ_α is just a constant that specifies the detector's location at the time $t = 0$. We set the initial phase $\phi_\alpha = -20°$ for LISA and $\phi_\alpha = 20°$ for Taiji. The orbits of the unit vectors of detector arms (two arms only) for LISA and Taiji are [93]

$$\begin{aligned}
\hat{u}_x &= -\sin(\bar{\phi}(t))\cos(\alpha_0(t)) + \cos(\bar{\phi}(t))\sin(\alpha_0(t))/2,\\
\hat{u}_y &= \cos(\bar{\phi}(t))\cos(\alpha_0(t)) + \sin(\bar{\phi}(t))\sin(\alpha_0(t))/2,\\
\hat{u}_z &= \sin(\pi/3)\sin(\alpha_0(t)),\\
\hat{v}_x &= -\sin(\bar{\phi}(t))\cos(\alpha_1(t)) + \cos(\bar{\phi}(t))\sin(\alpha_1(t))/2,\\
\hat{v}_y &= \cos(\bar{\phi}(t))\cos(\alpha_1(t)) + \sin(\bar{\phi}(t))\sin(\alpha_1(t))/2,\\
\hat{v}_z &= \sin(\pi/3)\sin(\alpha_1(t)),
\end{aligned} \tag{A2}$$

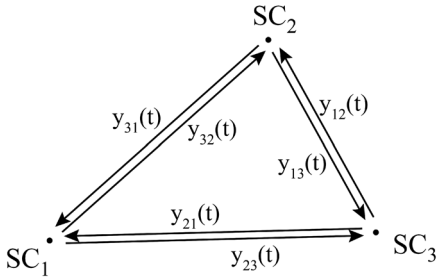

FIG. 11. Six data beams $y_{ab}(t)$ exchanged between the spacecrafts.

where $\alpha_i(t)$ increases linearly with time,

$$\alpha_i(t) = 2\pi t/T - \pi/12 - (i-1)\pi/3. \tag{A3}$$

APPENDIX B: TDI FOR SPACE-BASED GW ANTENNA

Following [79], we show the relative frequency fluctuations time series y_{ab} measured from detector SC_d to detector SC_b in Fig. 11. In the long-wavelength limit, we get the GW response for the six TDI signal

$$y_{ab}(t) = -\frac{1}{2}\sum_{ij}\hat{n}_a^i\hat{n}_a^j e_{ij}^A h_A(t), \tag{B1}$$

where $\hat{n}_a$ is the unit vector along the arm. The Michelson variable X uses only four beams and two laser beams exchanged between two of the SC_s. The GW response for X is

$$\begin{aligned}
X = {} & y_{32,322} - y_{23,233} + y_{31,22} - y_{21,33} + y_{23,2} - y_{32,3}\\
& + y_{21} - y_{31} + n(t),
\end{aligned} \tag{B2}$$

where the delayed data streams, e.g. $y_{23,2} = y_{23}(t - L_2)$, $y_{21,33} = y_{21}(t - L_3 - L_3)$. The noise in TDI combination X is

$$\begin{aligned}
S_n = {} & [8\sin^2(4\pi fL) + 32\sin^2(2\pi fL)]S_x/L^2\\
& + 16\sin^2(2\pi fL)S_a(2\pi f)^{-4}/L^2,
\end{aligned} \tag{B3}$$

The signal in Eq. (B2) can be rewritten as

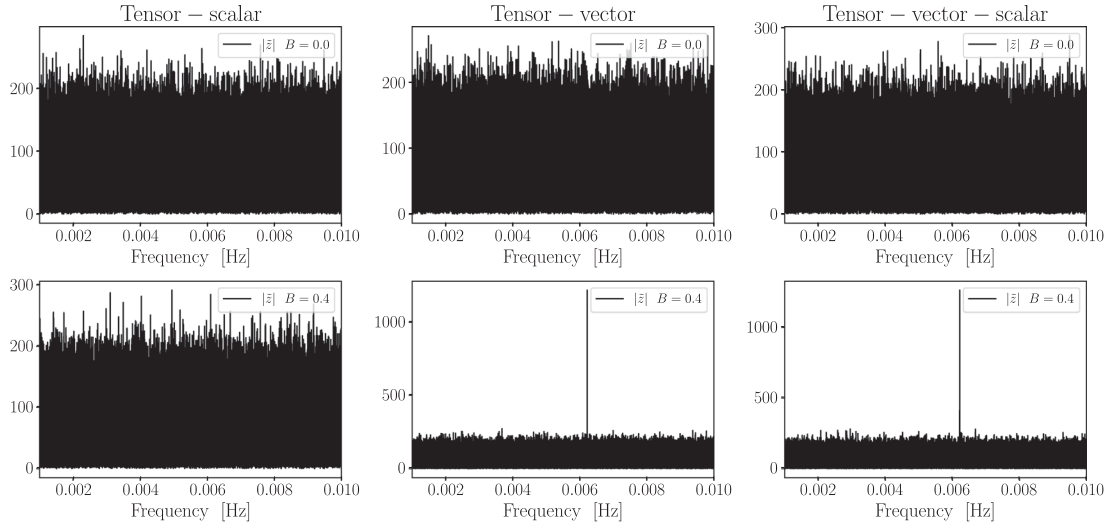

FIG. 12. The TDI combination X results of the null stream $|\tilde{z}|$ for the source J0806.3 + 1527 with LISA in the tensor-scalar (left panel), tensor-vector (middle panel), and tensor-vector-scalar (right panel) models.

$$d(t) = \bar{h}_+ F^+(\hat{\omega}, f_0, t) e^{2\pi i f_0 t + i\phi_D(t)} + \bar{h}_\times F^\times(\hat{\omega}, f_0, t) e^{2\pi i f_0 t + i\phi_D(t)} + n(t), \quad \text{(B4)}$$

where

$$\bar{h}_+ = \mathcal{A}[1+\cos^2(\iota)][e^{i\phi_0} + e^{i(\phi_0 - 2\pi f_0 L)} - e^{i(\phi_0 - 4\pi f_0 L)} - e^{i(\phi_0 - 6\pi f_0 L)}],$$
$$\bar{h}_\times = 2i\mathcal{A}\cos(\iota)[e^{i\phi_0} + e^{i(\phi_0 - 2\pi f_0 L)} - e^{i(\phi_0 - 4\pi f_0 L)} - e^{i(\phi_0 - 6\pi f_0 L)}].$$

Following the procedure discussed in Sec. III A, we inject a set of mock waveforms with $B = \{0, 0.4\}$ in addition to simulated signals from GR. The results for the tensor-scalar, tensor-vector and tensor-vector-scalar models with LISA are shown in Fig. 12. With $B = 0.4$ and a one year observation time, we get $\{\rho < 7, \rho = 31, \rho = 32\}$ for LISA in the tensor-scalar, tensor-vector, and tensor-vector-scalar models, respectively. These results are similar to those found in Sec. III A.

[1] B. P. Abbott *et al.* (LIGO Scientific, Virgo Collaborations), Observation of Gravitational Waves from a Binary Black Hole Merger, Phys. Rev. Lett. **116**, 061102 (2016).

[2] B. P. Abbott *et al.* (LIGO Scientific, Virgo Collaborations), GW150914: The Advanced LIGO Detectors in the Era of First Discoveries, Phys. Rev. Lett. **116**, 131103 (2016).

[3] B. P. Abbott *et al.* (LIGO Scientific, Virgo Collaborations), GW151226: Observation of Gravitational Waves from a 22-Solar-Mass Binary Black Hole Coalescence, Phys. Rev. Lett. **116**, 241103 (2016).

[4] B. P. Abbott *et al.* (LIGO Scientific, VIRGO Collaborations), GW170104: Observation of a 50-Solar-Mass Binary Black Hole Coalescence at Redshift 0.2, Phys. Rev. Lett. **118**, 221101 (2017); **121**, 129901(E) (2018).

[5] B. P. Abbott *et al.* (LIGO Scientific, Virgo Collaborations), GW170814: A Three-Detector Observation of Gravitational Waves from a Binary Black Hole Coalescence, Phys. Rev. Lett. **119**, 141101 (2017).

[6] B. P. Abbott *et al.* (LIGO Scientific, Virgo Collaborations), GW170817: Observation of Gravitational Waves from a Binary Neutron Star Inspiral, Phys. Rev. Lett. **119**, 161101 (2017).

[7] B. P. Abbott *et al.* (LIGO Scientific, Virgo Collaborations), GW170608: Observation of a 19-solar-mass binary black hole coalescence, Astrophys. J. Lett. **851**, L35 (2017).

[8] B. P. Abbott *et al.* (LIGO Scientific, Virgo Collaborations), GWTC-1: A Gravitational-Wave Transient Catalog of Compact Binary Mergers Observed by LIGO and Virgo during the First and Second Observing Runs, Phys. Rev. X **9**, 031040 (2019).

[9] B. P. Abbott *et al.* (LIGO Scientific, Virgo Collaborations), GW190425: Observation of a compact binary coalescence with total mass $\sim 3.4\ M_\odot$, Astrophys. J. Lett. **892**, L3 (2020).

[10] R. Abbott *et al.* (LIGO Scientific, Virgo Collaborations), GW190412: Observation of a binary-black-hole coalescence with asymmetric masses, Phys. Rev. D **102**, 043015 (2020).

[11] R. Abbott *et al.* (LIGO Scientific, Virgo Collaborations), GW190814: Gravitational waves from the coalescence of a 23 solar mass black hole with a 2.6 solar mass compact object, Astrophys. J. Lett. **896**, L44 (2020).

[12] R. Abbott *et al.* (LIGO Scientific, Virgo Collaborations), GW190521: A Binary Black Hole Merger with a Total Mass of 150 $M_\odot$, Phys. Rev. Lett. **125**, 101102 (2020).

[13] R. Abbott *et al.* (LIGO Scientific, Virgo Collaborations), GWTC-2: Compact Binary Coalescences Observed by LIGO and Virgo During the First Half of the Third Observing Run, Phys. Rev. X **11**, 021053 (2021).

[14] R. Abbott *et al.* (LIGO Scientific, VIRGO Collaborations), GWTC-2.1: Deep extended catalog of compact binary coalescences observed by LIGO and Virgo during the first half of the third observing run, arXiv:2108.01045.

[15] G. M. Harry (LIGO Scientific Collaboration), Advanced LIGO: The next generation of gravitational wave detectors, Classical Quantum Gravity **27**, 084006 (2010).

[16] J. Aasi *et al.* (LIGO Scientific Collaboration), Advanced LIGO, Classical Quantum Gravity **32**, 074001 (2015).

[17] B. P. Abbott *et al.* (LIGO Scientific, Virgo Collaborations), Tests of General Relativity with GW170817, Phys. Rev. Lett. **123**, 011102 (2019).

[18] D. M. Eardley, D. L. Lee, A. P. Lightman, R. V. Wagoner, and C. M. Will, Gravitational-Wave Observations as a Tool for Testing Relativistic Gravity, Phys. Rev. Lett. **30**, 884 (1973).

[19] D. M. Eardley, D. L. Lee, and A. P. Lightman, Gravitational-wave observations as a tool for testing relativistic gravity, Phys. Rev. D **8**, 3308 (1973).

[20] C. Brans and R. H. Dicke, Mach's principle and a relativistic theory of gravitation, Phys. Rev. **124**, 925 (1961).

[21] D. Liang, Y. Gong, S. Hou, and Y. Liu, Polarizations of gravitational waves in $f(R)$ gravity, Phys. Rev. D **95**, 104034 (2017).

[22] S. Hou, Y. Gong, and Y. Liu, Polarizations of gravitational waves in Horndeski theory, Eur. Phys. J. C **78**, 378 (2018).

[23] Y. Gong, S. Hou, E. Papantonopoulos, and D. Tzortzis, Gravitational waves and the polarizations in Hořava gravity after GW170817, Phys. Rev. D **98**, 104017 (2018).

[24] Y. Gong, S. Hou, D. Liang, and E. Papantonopoulos, Gravitational waves in Einstein-æther and generalized

TeVeS theory after GW170817, Phys. Rev. D **97**, 084040 (2018).
[25] T. Jacobson and D. Mattingly, Einstein-Aether waves, Phys. Rev. D **70**, 024003 (2004).
[26] K. Lin, X. Zhao, C. Zhang, T. Liu, B. Wang, S. Zhang, X. Zhang, W. Zhao, T. Zhu, and A. Wang, Gravitational waveforms, polarizations, response functions, and energy losses of triple systems in Einstein-aether theory, Phys. Rev. D **99**, 023010 (2019).
[27] C. Zhang, X. Zhao, A. Wang, B. Wang, K. Yagi, N. Yunes, W. Zhao, and T. Zhu, Gravitational waves from the quasicircular inspiral of compact binaries in Einstein-aether theory, Phys. Rev. D **101**, 044002 (2020); **104**, 069905(E) (2021).
[28] J. D. Bekenstein, Relativistic gravitation theory for the MOND paradigm, Phys. Rev. D **70**, 083509 (2004); **71**, 069901(E) (2005).
[29] F. Acernese *et al.* (VIRGO Collaboration), Advanced Virgo: A second-generation interferometric gravitational wave detector, Classical Quantum Gravity **32**, 024001 (2015).
[30] K. Somiya (KAGRA Collaboration), Detector configuration of KAGRA: The Japanese cryogenic gravitational-wave detector, Classical Quantum Gravity **29**, 124007 (2012).
[31] Y. Aso, Y. Michimura, K. Somiya, M. Ando, O. Miyakawa, T. Sekiguchi, D. Tatsumi, and H. Yamamoto (KAGRA Collaboration), Interferometer design of the KAGRA gravitational wave detector, Phys. Rev. D **88**, 043007 (2013).
[32] Y. Hagihara, N. Era, D. Iikawa, and H. Asada, Probing gravitational wave polarizations with Advanced LIGO, Advanced Virgo and KAGRA, Phys. Rev. D **98**, 064035 (2018).
[33] Y. Hagihara, N. Era, D. Iikawa, A. Nishizawa, and H. Asada, Constraining extra gravitational wave polarizations with Advanced LIGO, Advanced Virgo and KAGRA and upper bounds from GW170817, Phys. Rev. D **100**, 064010 (2019).
[34] P. T. H. Pang, R. K. L. Lo, I. C. F. Wong, T. G. F. Li, and C. Van Den Broeck, Generic searches for alternative gravitational wave polarizations with networks of interferometric detectors, Phys. Rev. D **101**, 104055 (2020).
[35] A. Nishizawa, A. Taruya, K. Hayama, S. Kawamura, and M.-a. Sakagami, Probing non-tensorial polarizations of stochastic gravitational-wave backgrounds with ground-based laser interferometers, Phys. Rev. D **79**, 082002 (2009).
[36] T. Callister, A. S. Biscoveanu, N. Christensen, M. Isi, A. Matas, O. Minazzoli, T. Regimbau, M. Sakellariadou, J. Tasson, and E. Thrane, Polarization-Based Tests of Gravity with the Stochastic Gravitational-Wave Background, Phys. Rev. X **7**, 041058 (2017).
[37] B. P. Abbott *et al.* (LIGO Scientific, Virgo Collaborations), Search for Tensor, Vector, and Scalar Polarizations in the Stochastic Gravitational-Wave Background, Phys. Rev. Lett. **120**, 201102 (2018).
[38] A. Nishizawa, A. Taruya, and S. Kawamura, Cosmological test of gravity with polarizations of stochastic gravitational waves around 0.1–1 Hz, Phys. Rev. D **81**, 104043 (2010).
[39] M. Isi, A. J. Weinstein, C. Mead, and M. Pitkin, Detecting beyond-Einstein polarizations of continuous gravitational waves, Phys. Rev. D **91**, 082002 (2015).
[40] M. Isi, M. Pitkin, and A. J. Weinstein, Probing dynamical gravity with the polarization of continuous gravitational waves, Phys. Rev. D **96**, 042001 (2017).
[41] B. P. Abbott *et al.* (LIGO Scientific, Virgo Collaborations), First Search for Nontensorial Gravitational Waves from Known Pulsars, Phys. Rev. Lett. **120**, 031104 (2018).
[42] L. O'Beirne, N. J. Cornish, S. J. Vigeland, and S. R. Taylor, Constraining alternative polarization states of gravitational waves from individual black hole binaries using pulsar timing arrays, Phys. Rev. D **99**, 124039 (2019).
[43] K. Hayama and A. Nishizawa, Model-independent test of gravity with a network of ground-based gravitational-wave detectors, Phys. Rev. D **87**, 062003 (2013).
[44] I. Di Palma and M. Drago, Estimation of the gravitational wave polarizations from a nontemplate search, Phys. Rev. D **97**, 023011 (2018).
[45] H. Takeda, A. Nishizawa, Y. Michimura, K. Nagano, K. Komori, M. Ando, and K. Hayama, Polarization test of gravitational waves from compact binary coalescences, Phys. Rev. D **98**, 022008 (2018).
[46] H. Takeda, A. Nishizawa, K. Nagano, Y. Michimura, K. Komori, M. Ando, and K. Hayama, Prospects for gravitational-wave polarization tests from compact binary mergers with future ground-based detectors, Phys. Rev. D **100**, 042001 (2019).
[47] M. Vallisneri, Use and abuse of the Fisher information matrix in the assessment of gravitational-wave parameter-estimation prospects, Phys. Rev. D **77**, 042001 (2008).
[48] L. Wen and Y. Chen, Geometrical expression for the angular resolution of a network of gravitational-wave detectors, Phys. Rev. D **81**, 082001 (2010).
[49] B. P. Abbott *et al.* (KAGRA, LIGO Scientific, Virgo, VIRGO Collaborations), Prospects for observing and localizing gravitational-wave transients with Advanced LIGO, Advanced Virgo and KAGRA, Living Rev. Relativity **21**, 3 (2018).
[50] K. Grover, S. Fairhurst, B. F. Farr, I. Mandel, C. Rodriguez, T. Sidery, and A. Vecchio, Comparison of gravitational wave detector network sky localization approximations, Phys. Rev. D **89**, 042004 (2014).
[51] C. P. L. Berry *et al.*, Parameter estimation for binary neutron-star coalescences with realistic noise during the Advanced LIGO era, Astrophys. J. **804**, 114 (2015).
[52] L. P. Singer and L. R. Price, Rapid Bayesian position reconstruction for gravitational-wave transients, Phys. Rev. D **93**, 024013 (2016).
[53] B. Bécsy, P. Raffai, N. J. Cornish, R. Essick, J. Kanner, E. Katsavounidis, T. B. Littenberg, M. Millhouse, and S. Vitale, Parameter estimation for gravitational-wave bursts with the BayesWave pipeline, Astrophys. J. **839**, 15 (2017).
[54] W. Zhao and L. Wen, Localization accuracy of compact binary coalescences detected by the third-generation gravitational-wave detectors and implication for cosmology, Phys. Rev. D **97**, 064031 (2018).
[55] C. Mills, V. Tiwari, and S. Fairhurst, Localization of binary neutron star mergers with second and third generation gravitational-wave detectors, Phys. Rev. D **97**, 104064 (2018).

[56] S. Fairhurst, Localization of transient gravitational wave sources: Beyond triangulation, Classical Quantum Gravity **35**, 105002 (2018).
[57] Y. Fujii, T. Adams, F. Marion, and R. Flaminio, Fast localization of coalescing binaries with a heterogeneous network of advanced gravitational wave detectors, Astropart. Phys. **113**, 1 (2019).
[58] C. Liu, W.-H. Ruan, and Z.-K. Guo, Constraining gravitational-wave polarizations with Taiji, Phys. Rev. D **102**, 124050 (2020).
[59] C. Zhang, Y. Gong, H. Liu, B. Wang, and C. Zhang, Sky localization of space-based gravitational wave detectors, Phys. Rev. D **103**, 103013 (2021).
[60] C. Zhang, Y. Gong, B. Wang, and C. Zhang, Accuracy of parameter estimations with a spaceborne gravitational wave observatory, Phys. Rev. D **103**, 104066 (2021).
[61] C. Zhang, Y. Gong, and C. Zhang, Parameter estimation for space-based gravitational wave detectors with ringdown signals, Phys. Rev. D **104**, 083038 (2021).
[62] Y. Gong, J. Luo, and B. Wang, Concepts and status of Chinese space gravitational wave detection projects, Nat. Astron. **5**, 881 (2021).
[63] K. Danzmann, LISA: An ESA cornerstone mission for a gravitational wave observatory, Classical Quantum Gravity **14**, 1399 (1997).
[64] P. Amaro-Seoane *et al.* (LISA Collaboration), Laser interferometer space antenna, arXiv:1702.00786.
[65] J. Luo *et al.* (TianQin Collaboration), TianQin: A spaceborne gravitational wave detector, Classical Quantum Gravity **33**, 035010 (2016).
[66] W.-R. Hu and Y.-L. Wu, The Taiji program in space for gravitational wave physics and the nature of gravity, Natl. Sci. Rev. **4**, 685 (2017).
[67] Y. Guersel and M. Tinto, Near optimal solution to the inverse problem for gravitational wave bursts, Phys. Rev. D **40**, 3884 (1989).
[68] S. Chatterji, A. Lazzarini, L. Stein, P. J. Sutton, A. Searle, and M. Tinto, Coherent network analysis technique for discriminating gravitational-wave bursts from instrumental noise, Phys. Rev. D **74**, 082005 (2006).
[69] L. J. Rubbo, N. J. Cornish, and O. Poujade, Forward modeling of space borne gravitational wave detectors, Phys. Rev. D **69**, 082003 (2004).
[70] F. B. Estabrook and H. D. Wahlquist, Response of Doppler spacecraft tracking to gravitational radiation, Gen. Relativ. Gravit. **6**, 439 (1975).
[71] N. J. Cornish and S. L. Larson, Space missions to detect the cosmic gravitational wave background, Classical Quantum Gravity **18**, 3473 (2001).
[72] M. Tinto and J. W. Armstrong, Cancellation of laser noise in an unequal-arm interferometer detector of gravitational radiation, Phys. Rev. D **59**, 102003 (1999).
[73] J. W. Armstrong, F. B. Estabrook, and M. Tinto, Time-delay interferometry for space-based gravitational wave searches, Astrophys. J. **527**, 814 (1999).
[74] S. L. Larson, W. A. Hiscock, and R. W. Hellings, Sensitivity curves for spaceborne gravitational wave interferometers, Phys. Rev. D **62**, 062001 (2000).
[75] S. L. Larson, R. W. Hellings, and W. A. Hiscock, Unequal arm space borne gravitational wave detectors, Phys. Rev. D **66**, 062001 (2002).
[76] M. Tinto and M. E. da Silva Alves, LISA sensitivities to gravitational waves from relativistic metric theories of gravity, Phys. Rev. D **82**, 122003 (2010).
[77] A. Blaut, Angular and frequency response of the gravitational wave interferometers in the metric theories of gravity, Phys. Rev. D **85**, 043005 (2012).
[78] D. Liang, Y. Gong, A. J. Weinstein, C. Zhang, and C. Zhang, Frequency response of space-based interferometric gravitational-wave detectors, Phys. Rev. D **99**, 104027 (2019).
[79] C. Zhang, Q. Gao, Y. Gong, D. Liang, A. J. Weinstein, and C. Zhang, Frequency response of time-delay interferometry for space-based gravitational wave antenna, Phys. Rev. D **100**, 064033 (2019).
[80] C. Zhang, Q. Gao, Y. Gong, B. Wang, A. J. Weinstein, and C. Zhang, Full analytical formulas for frequency response of space-based gravitational wave detectors, Phys. Rev. D **101**, 124027 (2020).
[81] B. Allen, W. G. Anderson, P. R. Brady, D. A. Brown, and J. D. E. Creighton, FINDCHIRP: An algorithm for detection of gravitational waves from inspiraling compact binaries, Phys. Rev. D **85**, 122006 (2012).
[82] T. Robson, N. J. Cornish, and C. Liu, The construction and use of LISA sensitivity curves, Classical Quantum Gravity **36**, 105011 (2019).
[83] X.-C. Hu, X.-H. Li, Y. Wang, W.-F. Feng, M.-Y. Zhou, Y.-M. Hu, S.-C. Hu, J.-W. Mei, and C.-G. Shao, Fundamentals of the orbit and response for TianQin, Classical Quantum Gravity **35**, 095008 (2018).
[84] W.-H. Ruan, Z.-K. Guo, R.-G. Cai, and Y.-Z. Zhang, Taiji program: Gravitational-wave sources, Int. J. Mod. Phys. A **35**, 2050075 (2020).
[85] G. L. Israel *et al.*, Rxj0806.3 + 1527: A double degenerate binary with the shortest known orbital period (321s), Astron. Astrophys. **386**, L13 (2002).
[86] S. C. C. Barros, T. R. Marsh, P. Groot, G. Nelemans, G. Ramsay, G. Roelofs, D. Steeghs, and J. Wilms, Geometrical constraints upon the unipolar model of V407 Vul and RX J0806.3 + 1527, Mon. Not. R. Astron. Soc. **357**, 1306 (2005).
[87] G. H. A. Roelofs, A. Rau, T. R. Marsh, D. Steeghs, P. J. Groot, and G. Nelemans, Spectroscopic evidence for a 5.4-minute orbital period in HM Cancri, Astrophys. J. Lett. **711**, L138 (2010).
[88] P. Esposito, G. L. Israel, S. Dall'Osso, and S. Covino, Swift X-ray and ultraviolet observations of the shortest orbital period double-degenerate system RX J0806.3 + 1527 (HM Cnc), Astron. Astrophys. **561**, A117 (2014).
[89] T. Kupfer, V. Korol, S. Shah, G. Nelemans, T. R. Marsh, G. Ramsay, P. J. Groot, D. T. H. Steeghs, and E. M. Rossi, LISA verification binaries with updated distances from Gaia Data Release 2, Mon. Not. R. Astron. Soc. **480**, 302 (2018).
[90] P. J. Sutton *et al.*, X-Pipeline: An analysis package for autonomous gravitational-wave burst searches, New J. Phys. **12**, 053034 (2010).

[91] K. Chatziioannou, N. Yunes, and N. Cornish, Model-independent test of general relativity: An extended post-Einsteinian framework with complete polarization content, Phys. Rev. D **86**, 022004 (2012); **95**, 129901(E) (2017).

[92] C. J. Moore, R. H. Cole, and C. P. L. Berry, Gravitational-wave sensitivity curves, Classical Quantum Gravity **32**, 015014 (2015).

[93] C. Cutler and A. Vecchio, LISA's angular resolution for monochromatic sources, AIP Conf. Proc. **456**, 95 (1998).